Effect of current density on the Li – Li_6PS_5Cl solid electrolyte interphase

Sudarshan Narayanan[a,b], Ulderico Ulissi[c], Joshua S. Gibson[a,b], Yvonne A. Chart[a,b], Robert S. Weatherup[a,b], and Mauro Pasta[a,b,*]

[a]Department of Materials, University of Oxford, Parks Road, Oxford OX1 3PH, United Kingdom
[b]The Faraday Institution Quad One, Harwell Science and Innovation Campus, Didcot OX11 0RA, U.K.
[c]Nissan Technical Centre Europe, Moulsoe Road, Cranfield Technology Park, Bedford MK43 0DB, U.K.

[*]Corresponding author: mauro.pasta@materials.ox.ac.uk

Abstract

Understanding the nature and evolution of interphasial products at the Li metal – solid electrolyte interface is crucial in solid-state lithium batteries (SSBs). Using operando X-ray photoelectron spectroscopy and electrochemical impedance spectroscopy, we highlight the role of lithium plating current density on the evolution of the Li_6PS_5Cl–Li solid electrolyte interphase (SEI) composition in a "lithium-free" anode configuration. We conclude that higher current densities facilitate the formation of a more uniform, Li_3P-rich SEI thereby decreasing the electrode-electrolyte interfacial impedance. This study improves understanding of the role of plating kinetics in lithium-free SSBs and suggests a new strategy to modulate electrode-electrolyte interphases to achieve more efficient lithium plating.

Solid state battery (SSB) technology is fast becoming an attractive option to power electric vehicles (EVs), primarily as it can enable the safe implementation of lithium metal anodes (theoretical capacity $\sim$3860 mAh·g^{-1} and 2061 mAh·cm^{-3}). These can lead to cells with gravimetric and volumetric energies upwards of 400 Wh·Kg^{-1} and 1000 Wh·L^{-1}, which are thermally stable and also amenable to fast charging.[1–4] However, Li metal adoption is fraught with issues that hinder its commercialisation. With a strong reduction potential of –3.04 V (vs. standard hydrogen electrode), Li typically reacts with solid electrolytes (SEs) to form kinetically and thermodynamically unstable interphases. Combined with other morphological, structural, and chemo-mechanical processes at the Li-SE interface, gradual cell performance degradation and failure follows as a consequence of poor electrode-electrolyte contact, current focusing,

mechanical fracture of the SE, inhomogeneous plating/stripping, Li filamentary growth, and void formation.[5–9]

Despite possessing a limited electrochemical stability window[10], the Li_6PS_5Cl (LPSCl) electrolyte is known to form a kinetically stable solid electrolyte interphase (SEI) when in contact with metallic Li.[7, 11] While on one hand the formation of this SEI is necessary to prevent further SE decomposition, on the other it negatively impacts the electrochemical performance of the SSB as it significantly increases the interfacial impedance.[12–14] Specifically for LPSCl, the decomposition products are Li_2S, LiCl, and Li_xP, which are poor Li$^+$ ion conductors ($\sigma < 10^{-7}$ S·cm^{-1})[15] and directly affect cycling capacities and coulombic efficiencies at anodic potentials.[16, 17] Based on thermodynamic considerations, it has been postulated that Li_6PS_5Cl decomposes

1

via a multi-step mechanism that can broadly be represented by $Li_6PS_5Cl \rightarrow Li_2S + P + LiCl \rightarrow Li_3P$, transitioning through partially reduced phosphide species that are typically formed under Li-deficient conditions.[18–20] Interestingly, the fully reduced Li_3P has been shown to have an ionic conductivity of $\sigma > 10^{-4}$ S·cm^{-1} at room temperature, while also demonstrating good stability in contact with Li metal.[15, 21]

Such insights into interfacial degradation phenomena can inform improved engineering of interfaces that are stable even at high current densities. Previously, the use of anode interlayers, Li alloys, and high stack pressures have been proposed as solutions towards durable cycling at extreme rates, albeit at the cost of reduced energy density and/or scalability.[22–24] Recently, a novel technique employing the use of electrochemical pulses has been reported as a means to decrease interfacial impedance between Li metal and oxide SEs that typically form kinetically and thermodynamically stable interphases, through improved Li–SE contact[25]. Although such interfacial reduction processes are understood to be mainly controlled by reaction kinetics[11, 26, 27], a systematic investigation of their effects, especially at the Li-SE interface, is still missing. In particular, the evolution of the Li–LPSCl SEI itself as a function of Li metal plating/stripping kinetics is poorly understood.[28]

Here we investigate a current density-mediated evolution of the interphase formed between Li metal and LPSCl sulphide solid electrolyte during electrochemical plating using an operando X-ray photoemission spectroscopy (XPS) technique. Correlating these results with electrochemical impedance spectroscopy (EIS) analysis of this process in a "lithium-free" negative electrode solid-state configuration further provides valuable insights into the impact of SEI formation kinetics and composition on the Li–SE interfacial impedance. These findings can support the development of novel formation protocols to engineer stable interfaces, thereby improving lithium plating and stripping efficiency at high current densities.

The choice of a lithium-free negative electrode configuration is the most suitable and relevant system to investigate the initial formation and subsequent evolution of the SEI. Furthermore, such a system is also attractive from the perspective of increased energy densities, Li-free processing and lower cost.[29] Owing to the dynamic nature of such interfaces, it is imperative that in situ and operando techniques are utilised to adequately characterise the system.[9] The aforementioned operando XPS method, illustrated schematically in Figure 1a, has been adapted from one that was previously developed and described in detail by Wood et al. and in other related works.[20, 30, 31] We also refer to this as a "virtual electrode plating" process throughout the rest of this study. This stems from the formation of a "virtual electrode" following exposure of a grounded and Li-backed SE surface to an electron beam. The negatively charged surface thus formed facilitates migration of Li$^+$ ions eventually leading to plating of metallic Li on the SE surface. Furthermore, in this study, the electron beam current (EBC) was adjusted to modulate the electron flux incident at the SE surface, hence tuning the virtual electrode plating current. To observe the electrochemical response due to the evolution of the interface, an effectively identical setup was used in a solid electrolyte cell (SS|SE|LiIn|SS) so as to study the plating of Li at a stainless steel (SS) current collector (CC) using impedance and potential analyses at various applied current densities (Figure 1b).

Results and Discussion

Virtual electrode plating in XPS and SEI evolution

Solid LPSCl pellets (diameter, $\varphi_s = 5$ mm) were first cold-pressed inside a glovebox, to which thin Li metal and stainless steel (SS) foils were attached as current collectors (CC) as shown in Figure 1a. The assembled pellets for operando XPS were then mounted on an XPS sample stage using conductive carbon tape (to ensure a conductive path to the grounded stage) with the exposed LPSCl surface facing the X-ray beam. Detailed experimental procedures can be found in the Methods section. With the EBC set to 30 μA, core-level photoemission spectra for Li 1s, S 2p, P 2p and Cl 2p transitions were acquired at 1 minute intervals, over a period of ∼18 mins. The Ar$^+$ charge neutralisation feature was turned off throughout the experiment. Additionally, spectra pertaining to oxygen and carbon, typically present as trace contaminants in inert gas and vacuum environments, were also collected, since these too provide useful insights into SEI evolution.[20, 32–34] Figure 2a (panel 1) shows the evolution of the Li 1s spectra as the virtual electrode plating
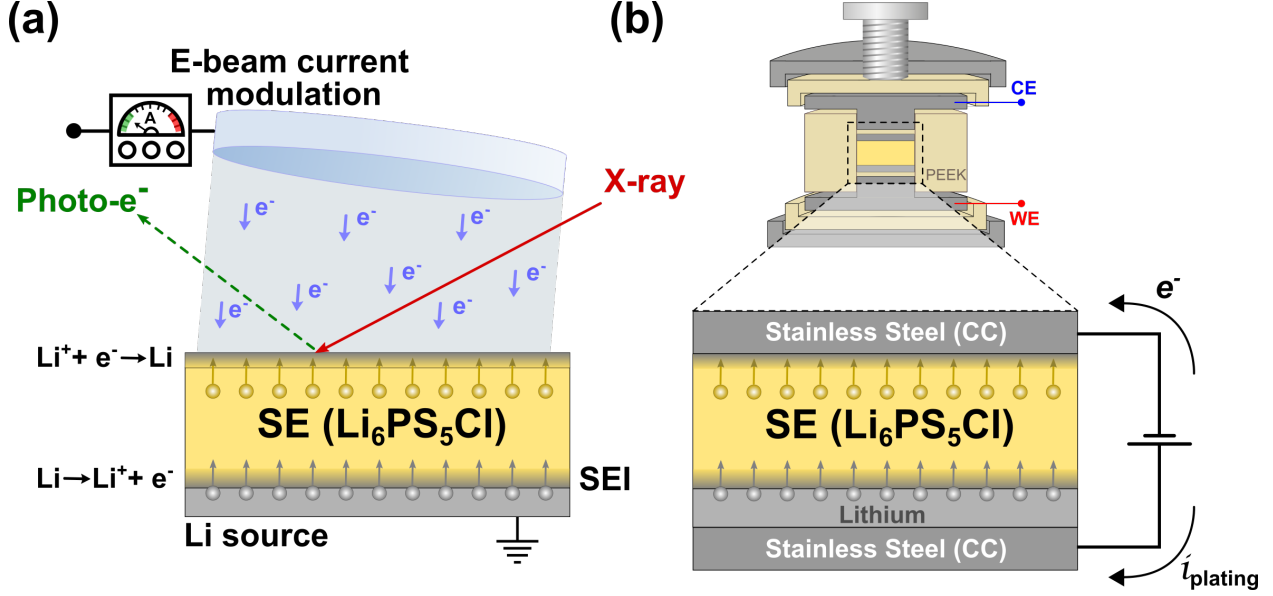
Figure 1. Schematics depicting (a) the operando XPS virtual electrode plating technique where the electron beam current can be modulated while acquiring photoemission spectra from the surface of the solid electrolyte (SE), and (b) the electrochemical setup in a lithium-free anode configuration for Li_6PS_5Cl SE for studying impedance and electrode potential evolution during plating at the Li-free electrode (stainless steel current collector).

progresses. Taking into account the size of the charge-neutralising e^--beam (diameter $\varphi_{e^-} \approx 5$ mm for the BaO electron neutraliser), an equivalent current density (j_{eq}) applied to the sample is defined here as $j_{eq} = EBC/a_s$, where a_s is the surface area (here, $a_s = a_{e-beam}$). Accordingly, the amount of Li plated can be estimated from j_{eq}, the time of exposure (t_{exp}), and expressed in terms of an equivalent areal charge passed, q_A, such that $q_A = j_{eq} \cdot j_{exp}$ ($\mu Ah \cdot cm^{-2}$).

At 30 μA EBC ($j_{eq} \approx 0.15$ $mA \cdot cm^{-2}$), the evolution of Li 1s spectra in the first panel of Figure 2a initially depicts a broadening of the peak followed by a gradual shift towards lower binding energies (B.E.). As mentioned earlier, during initial contact with LPSCl, Li metal forms Li_2S, Li_xP, and LiCl, along with other products from reactions with contaminants, such as Li_2O and Li_2CO_3. The peak-broadening observed here can be directly attributed to the formation of these interphasial products.[12, 33] Eventually, after the sample has been exposed to $q_A \approx 8.5$ $\mu Ah \cdot cm^{-2}$, a low B.E. peak appears around ~52.5 eV (coloured in blue) characteristic of metallic Li (Li^0) plating at the SE surface. This feature continues to grow in intensity

as plating proceeds. Evolution of the Li 1s spectra for the same plating process conducted at an EBC of 10 μA ($j_{eq} \approx 0.05$ $mA \cdot cm^{-2}$) is largely similar to that for $j_{eq} = 0.15$ $mA \cdot cm^{-2}$ (second panel of Figure 2a), except in the appearance and later growth of the low B.E. Li^0 peak. This feature grows in intensity more slowly than when plating at $j_{eq} = 0.15$ $mA \cdot cm^{-2}$, for approximately equivalent charge passed ($q_A > 12.8$ $\mu Ah \cdot cm^{-2}$). This disparity is amplified further on lowering the EBC to 2.5 μA ($j_{eq} \approx 0.01$ $mA \cdot cm^{-2}$), where only a negligible Li^0 peak is visible even after $q_A > 20$ $\mu Ah \cdot cm^{-2}$ of equivalent charge has been passed (third panel, Figure 2a). From a qualitative assessment of the Li 1s spectra, we infer that the formation and growth of a metallic Li layer occurs at $q_A < 10$ $\mu Ah \cdot cm^{-2}$ at higher current densities ($j_{eq} \geq 0.1$ $mA \cdot cm^{-2}$), while at lower current densities, the SEI continues to evolve.

To quantitatively interpret this observation, the Li 1s spectra were fitted to the following components (using Gaussian and Voigt lineshapes for the pristine LPSCl and SEI layers, and an asymmetric Doniach-Sunjic lineshape for Li metal) - (i) Li at the surface of the as-prepared LPSCl pellet, likely representing products of reaction with
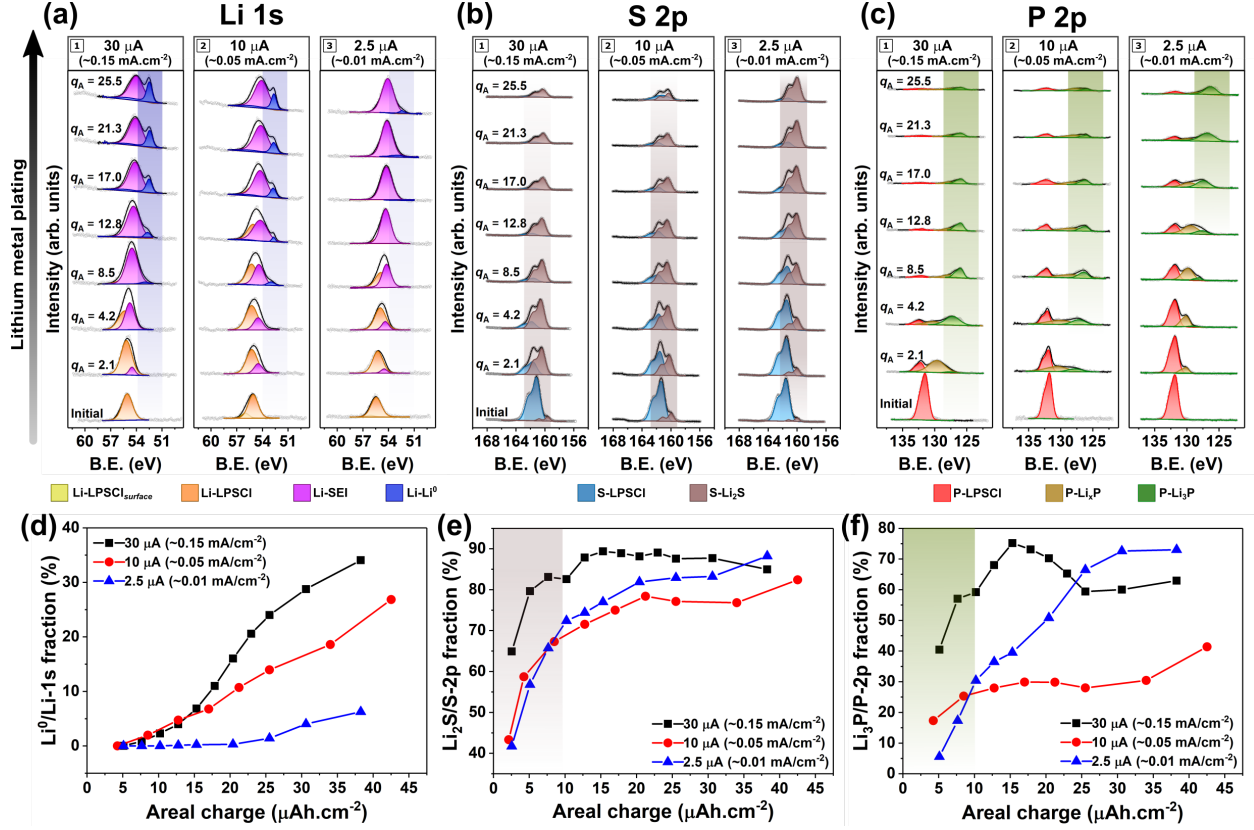
Figure 2. Evolution of core-level XPS spectra during the virtual electrode plating process at the LPSCl surface, at applied EBCs of 30 μA (or ~0.15 mA·cm^{-2}, panel 1), 10 μA (or ~0.05 mA·cm^{-2}, panel 2) and 2.5 μA (or ~0.01 mA·cm^{-2}, panel 3), for (a) Li 1s, (b) S 2p and (c) P 2p transitions, as a function of the charge passed, q_A (μAh·cm^{-2}). Quantification of XPS spectra plotted over varying amounts of charge passed at different current densities, depicting compositional fraction of (d) metallic Li (Li^0) in Li 1s, (e) Li$_2$S in S 2p, and (f) Li$_3$P in P 2p. A larger fraction of Li^0 and Li$_3$P for small amounts of charge passed at higher current densities indicates faster reaction kinetics at the interface resulting in a quicker formation and growth of a metallic Li layer during plating.

surface-adsorbed species, such as carbon, oxygen, CO_3^{2-}, HCO_3^-, OH^-, etc., (ii) Li-ions bound within the P-S tetrahedron of the Li_6PS_5Cl argyrodite structure, labelled as Li-LPSCl, (iii) Li-ions as part of the formed interphase, collectively identified as Li-SEI owing to the complexity in deconvoluting individual contributions, and (iv) metallic Li, marked as Li-Li^0.[12, 33] Comparing the fraction of metallic Li in the Li 1s spectra and its evolution as a function of the equivalent charge passed provides quantitative evidence for the accelerated appearance of a metallic Li layer at higher current densities (Figure 2d). In other words, we conclude that Li plates out as a metallic layer faster at higher current densities than at lower ones.

While the Li 1s spectra provides insights into Li plating behaviour, the S 2p and P 2p spectra shed light on the evolution of the SEI chemistry. In the case of the S 2p signal, as indicated in Figure 2b, with increasing amount of Li plated, a doublet feature characteristic of Li$_2$S (2p$_{3/2}$ B.E. ~160 eV, coloured in brown) develops, almost readily. This is a well reported and studied component of the Li–LPSCl SEI that forms even under Li-deficient conditions.[12, 20, 33] As the virtual electrode plating process progresses and metallic Li accumulates at the SE surface, the intensity of the Li$_2$S component diminishes owing to the limited depth sensitivity of XPS acquired with an Al Kα source (~ 1-5 nm). On close examination of the composition quantified

4

from spectra measured at the different EBCs as in Figure 2e, reduction of the LPSCl surface to Li_2S occurs at a noticeably faster rate at a higher j_{eq} (here, 0.15 mA·cm^{-2}). Even for low equivalent charge passed ($q_A \approx 5$ µAh·cm^{-2}), ~90% of the developing SEI comprises Li_2S. By comparison, at $j_{eq} \leq 0.05$ mA·cm^{-2}, only about 70% of the SE surface is composed of the reduced sulphide species. This indicates comparatively sluggish reaction kinetics at lower current densities driven by various reduction reactions competing for available reactant species (here, plated Li).

Meanwhile, phosphorous in the P-S tetrahedron has been reported to follow a less direct route towards reduction to Li_3P upon reaction with the plating Li by forming multiple partially reduced species, as discussed earlier, that are often collectively labelled as Li_xP.[18–20] Comparing evolution in the P 2p spectra reveals a swift reduction to a low B.E. doublet feature ($2p_{3/2} \approx 126$ eV) at the highest j_{eq}, for $q_A < 5$ µAh·cm^{-2} of equivalent charge passed (Figure 2c - panel 1, coloured in green), representative of the fully reduced Li_3P. In contrast, for $j_{eq} \leq 0.05$ mA·cm^{-2} at similar amounts of charge passed, the initial SEI formed more prominently comprises a broad spectral feature (126 eV $<$ B.E. $2p_{3/2} < 131$ eV) characteristic of the partially reduced Li_xP. Continued plating eventually results in the formation of the fully reduced Li_3P at lower current densities as well, accompanied by a large decrease in the overall P 2p spectral intensity, suggesting accumulation of plated metallic Li. These observations imply the formation of a Li_3P-rich SEI in the early stages of its formation for Li plated at high current densities even at low equivalent charge passed. The fraction of Li_3P quantified as a function of the equivalent charge passed, particularly for $q_A < 10$ µAh·cm^{-2} (Figure 2f) provides evidence supporting this conclusion. In Figures 2b-c, it can also be seen that XPS signal pertaining to pristine LPSCl components are more rapidly attenuated in intensity at higher j_{eq} for similar equivalent charge passed (for example, $q_A = 12.8$ µAh·cm^{-2}). With XPS spectra acquired over an area of 500 µm × 500 µm, representing a large sampling surface, it can be inferred that the SEI layer formed is comparatively more uniform and homogeneous for Li plated at higher current densities. We note that the suppression of P 2p photoemission signal with increased Li plating (Figure 2c), does result in a lower signal-to-noise ratio. Accordingly, subsequent errors in component fitting limit the validity of such a comparison of fitted components, especially of S and P, to low equivalent charge regimes ($q_A < 10$ µAh·cm^{-2}, highlighted regions in Figures 2e-f).

The partially reduced Li_xP species observed are not transient or metastable either. Figure S1 shows that the corresponding P 2p feature remains stable and largely unperturbed even after a 24 hour period when left under vacuum, inside the XPS. Also, the presence of the partially reduced phosphide buried under the surface of a ~20 nm Li layer thermally evaporated on the LPSCl surface, from spectra obtained using a tunable-energy synchrotron X-ray source, is further testament to the reactive stability of the species in the absence of an electrochemical plating/stripping event (Figure S2a-c). Although with passage of adequate charge the SEI is rendered self-limiting[7], evolution of the core-level XPS spectra for Li, S, and P indicate significant variations in the SEI composition itself for the virtual electrode plating conducted at j_{eq} ranging from high (0.15 mA·cm^{-2}) to low (0.01 mA·cm^{-2}). Plausible reasons to explain these observations could be twofold: (a) the inherent kinetics and energetics associated with the reaction between Li metal and sulphide SEs, and (b) the thermodynamics of nucleation and growth of Li metal at the SE surface governed by electrochemical overpotential and surface energy considerations.[11] While thermodynamic forces are no doubt crucial in understanding Li–SE interfacial evolution, we hypothesise that reaction kinetics play a dominant role in determining the SEI evolution phenomena observed in this work. This has important ramifications in the context of overall interfacial impedance of the cell which will be discussed in later sections.

Similar results were obtained on probing the SEI evolution at the Li–SE interface by in situ sputtering of Li[12], where the Li sputter rate was controlled by varying the Ar$^+$ ion acceleration voltage (Figure S3). However, since surface damage by the more energetic Li atoms produced by sputtering has been shown to affect interfacial reactions in a recent study by us[34], direct correlation of observed SEI evolution with varying flux of incident Li atoms is not feasible in such a setup. Another by-product of the reaction between Li and LPSCl is LiCl, which cannot be easily discerned using XPS owing to the binding energies of chlorine in both LPSCl and LiCl being nearly identical, as shown in Figure S4a.[12, 33, 35] Though an inevitable contaminant, the evolution of O 1s

spectra as a function of progression in the virtual electrode plating process also confirms the disparity in Li reaction kinetics, with the formation of Li_2O species (at a B.E. of $\sim$528.5 eV) proceeding at a faster rate for less equivalent charge passed at higher EBCs (see Figure S4b).

Electrochemical plating in cells with lithium-free anode

To evaluate the impact of current density dependent interphasial evolution on the electrochemical properties of the system, a solid-state half-cell (SS|LPSCl|LiIn|SS) in an "lithium-free" anode configuration was setup as described in the schematic in Figure 1b. Here, a LiIn alloy ($Li_{0.25}In_{0.75}$) was used as a source of Li owing to its known interfacial stability with sulphide SEs, thus allowing for isolation of changes occurring at the SS|LPSCl side.[22] Closely replicating the virtual electrode plating experiment in the XPS, the evolution of cell impedance was studied during plating of Li at the stainless steel (SS) ion-blocking electrode on the anode side by applying different current densities (identified here as $J_{0.01}$=0.01 mA·cm^{-2}, $J_{0.05}$=0.05 mA·cm^{-2}, $J_{0.5}$=0.5 mA·cm^{-2} and $J_{2.5}$=2.5 mA·cm^{-2}). The cells were allowed to stabilise over a period of 24-48 hours (see Figure S5a-b) prior to plating. As in the case of XPS spectra discussed earlier, the Nyquist plots also show marked differences in their evolution for equivalent amounts of charge passed, depending on the current density applied (Figures 3a-d). In particular, at relatively low current densities (J = 0.01-0.05 mA·cm^{-2} in this study), the low frequency tail of the impedance curves shows a gradual decrease in Re(Z) as Li plating proceeds. This is expected, owing to gradually improving contact between the Li metal and the LPSCl surface as Li plates. In contrast, at higher current densities ($J \geq$ 0.5mA·cm^{-2} in this study), for an equivalent amount of Li plated at the SS current collector, the same low frequency component of Re(Z) converges to a stable value faster, with this effect being most prominent at the highest tested current density, $J_{2.5}$.

Current density dependent evolution of interfacial impedance

In order to understand the underlying cause of this trend, the Nyquist plots obtained were fitted to the equivalent circuit schematically depicted in Figure 4a.[37] The variations in impedance can largely be attributed to the interface, which comprises the SEI and charge transfer (CT) components that are represented by the low frequency segment of the spectra.[37–39] The interfacial impedance can then be approximated as $R_{int} = R_{SEI} + R_{CT}$[37], where R_{CT} is related to the intrinsic kinetics of the system.[27, 40, 41] Indeed, a plot of combined resistances from SEI and CT contributions (Figure 4b) suggests that at low current densities (in this study, $J_{0.5}$ and $J_{0.05}$), the interfacial resistance asymptotically reaches a minima. In stark contrast, for Li plating conducted at a significantly higher current density ($J_{2.5}$), the interface attains the same minimum resistance almost as soon as Li begins plating. It is noteworthy that the differences in impedance evolution are most prominent over $\sim$50 µAh·cm^{-2} of charge passed, beyond which the effect diminishes as expected, while plating proceeds to form a metallic Li layer in both cases. Thus, a rapid drop in interfacial resistance, combined with the appearance of fully reduced reaction products (Li_3P in particular) and presence of a greater fraction of metallic Li in XPS analyses, all observed within $\sim$ 10 µAh·cm^{-2} of charge passed during initial stages of plating, strongly suggest the formation of a more uniform and homogeneous SEI layer as well, for Li plated at high current densities.

Recalling an earlier discussion on overpotential-dictated Li nucleation and growth behaviour during plating[11, 40, 42], overpotentials due to current density variations in this study were also measured (Figure S5c) but their contribution to the SEI evolution observed here are beyond the scope of this work and will be the subject of a future study. Meanwhile, the evolution of electrochemical impedance observed here in conjunction with that of SEI chemistry measured using the XPS validates the assumption of a kinetically mediated reaction process governing the Li–SE interface. This understanding is also in good agreement with previous reports that have shown, through finite element simulations, that the presence of a Li_3P membrane layer on the electrode surface results in a more homogeneous electric field distribution, enabling more uniform Li plating/stripping.[21] The validity of this hypothesis was experimentally verified by testing the utilisation efficiencies of the anodes formed in an identical lithium-free cell setup. The experiment involved plating Li at two current densities ($J_{0.05}$ and $J_{2.5}$) and then stripping both electrodes at the same
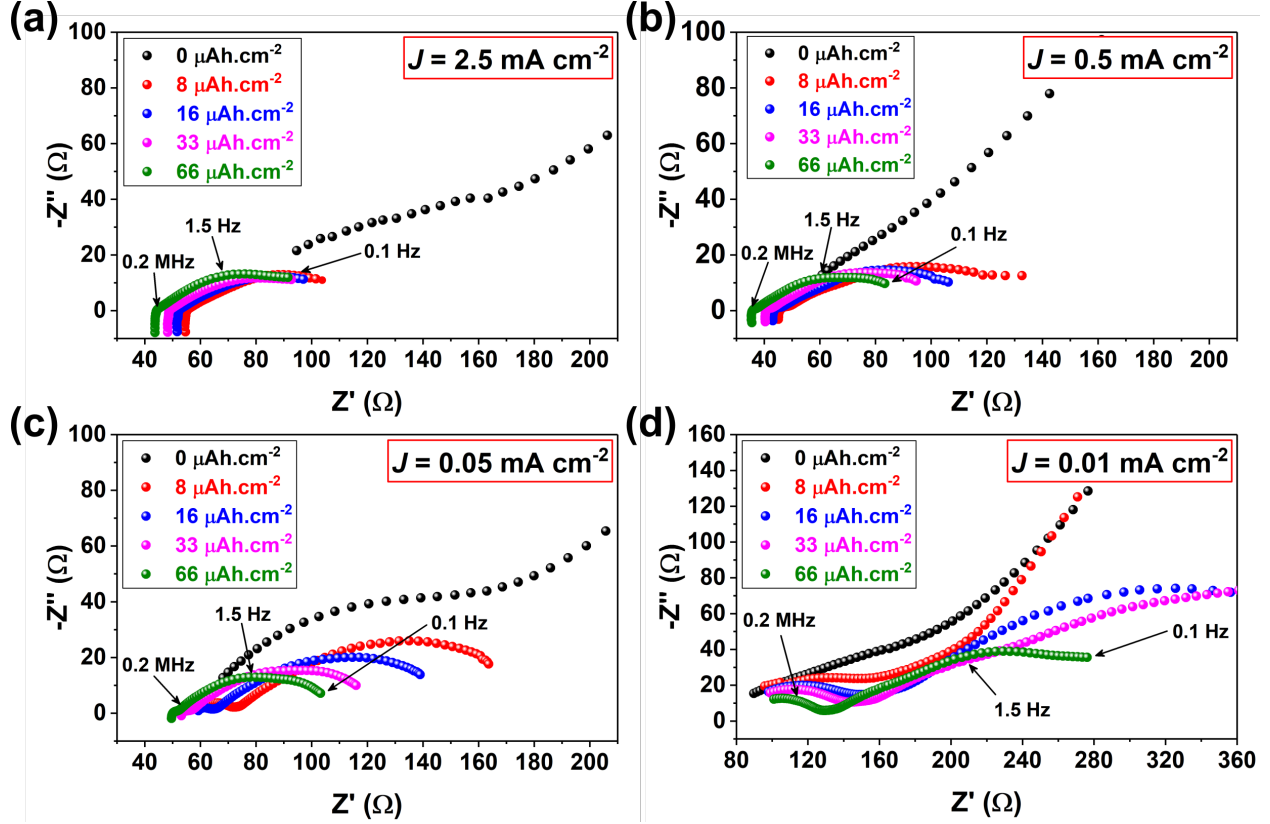
Figure 3. Nyquist curves depicting evolution of electrochemical impedances for the lithium-free half cell SS|LPSCl|LiIn|SS for plating at (a) $J_{2.5}$ =2.5 mA·cm^{-2}, (b) $J_{0.5}$ = 0.5 mA·cm^{-2}, (c) $J_{0.05}$ = 0.05 mA·cm^{-2}, and (d) $J_{0.01}$ = 0.01 mA·cm^{-2}, after passing similar equivalent charge. Variation in the low frequency tail of the impedance curves can be correlated to extent of change in interphasial evolution. The high impedance resulting from poor initial contact with the ion-blocking electrode at the Li-less anode side is evident from EIS curves at q_A = 0 µAh·cm^{-2}.[36]

current density ($J_{Stripping}$ = 0.25 mA·cm^{-2}). Figures S6a-b demonstrate that almost twice the amount of Li was successfully stripped out from the cell plated at a higher current density. An ex-situ examination of scanning electron micrographs (SEM) of the SS foil surface peeled off from the LPSCl surface, after passing $q_A \approx 30$ µAh·cm^{-2} of charge at $J_{2.5}$ and $J_{0.05}$ (Figures S7a and S6b respectively) reveals a pattern of Li islands covered with SE material adhered to them similar to that described by Schlenker et al.[38] Here, for the sample plated at $J_{2.5}$ the islands appear relatively smaller and more uniformly distributed spatially, supporting the argument of homogeneity in Li plating at higher current densities.

In conclusion, we report here a current density-mediated evolution of the interphase formed from contact of Li metal with an Li_6PS_5Cl SE introduced using an operando virtual electrode electrochemical plating method during XPS measurements, that suggests a significant role of reaction kinetics in these processes. At high current densities, in the initial stages of plating, this interphase was found to be rich in Li_3P, a fully reduced decomposition product of Li_6PS_5Cl. Evidenced by the appearance of metallic Li plated at the SE surface combined with the complete suppression of spectroscopic signal from the pristine LPSCl surface at relatively low equivalent charge passed, the interphase at high current densities is understood to be effectively more uniform as well. Analysis of interfacial impedances using EIS routines in conjunction with XPS spectra lend further credence to such an assertion. Moreover, the SEI formed at higher current densities, consisting of
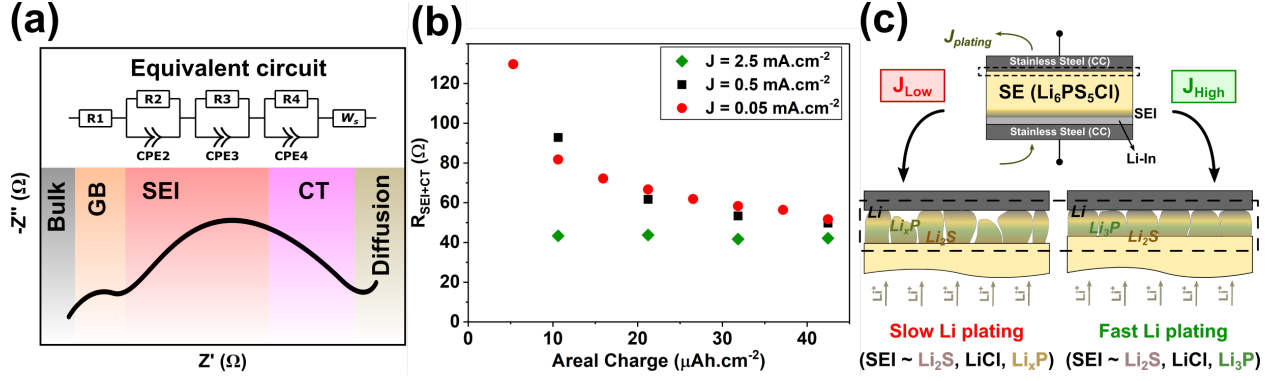
Figure 4. (a) Equivalent circuit used for fitting the EIS data along with a schematic describing the impedance contributions. (b) Variation in R_{int} ($R_{SEI} + R_{CT}$) from fitted EIS data as a function of amount of charge passed during Li plating at current densities, $J_{2.5} = 2.5$ mA·cm^{-2}, $J_{0.5} = 0.5$ mA·cm^{-2} and $J_{0.05} = 0.05$ mA·cm^{-2}.[37, 38] (c) Schematic representation of the likely mechanism of SEI formation and Li plating as a function of applied current density, at $J_{2.5}$ and $J_{0.05}$.

the Li$^+$ ion conducting Li$_3$P, is inferred to be more homogeneous. We believe this understanding can be leveraged to suitably engineer electrode-electrolyte interfaces and develop novel charge-discharge protocols, particularly in lithium-free SSBs that can enable more efficient utilisation of the anode, thereby improving cell cyclability and coulombic efficiencies.

Experimental section

Sample Preparation

Li$_6$PS$_5$Cl (LPSCl) argyrodite sulphide solid electrolyte powder was purchased from Ampcera™ (D50 $\sim$ 1 µm) through MSE Supplies LLC., and used as received. For operando XPS measurements, pellets of diameter 5mm ($\sim$25 mg to obtain $\sim$700-750 µm thick pellets) were cold-sintered using a hydraulic press, at 500 MPa for 5 mins. Li foil (30 µm thick) procured from Honjo Metal Co. Ltd. through KISCO GmbH was used as received and pressed onto one side of the LPSCl pellet mechanically by applying a pressure of $\sim$ 50-70 MPa, after punching out a 5mm diameter disc. Additionally, a 5mm diameter disc of stainless steel (SS316, 25µm thick, Advent Research Materials Ltd.) was pressed against the Li foil. The assembled stacks were then mounted onto the XPS stage using conductive carbon tape.

Sample stacks for electrochemical measurements were prepared by pressing solid electrolyte powder ($\sim$100 mg to obtain $\sim$700-750 µm thick pellets) within a 10 mm diameter polyether ether ketone

(PEEK) mould, along with an SS disc of the same size to be used as the plating electrode, using the same conditions as previously. Further, an alloy of LiIn, obtained by melt-processing lithium and indium metals in the atomic ratio 25:75, was calendared into a foil of thickness $\sim$50 µm. A disc of diamater 10mm punched out from this foil was then used as the other electrode, pressed with an SS current collector by application of pressure as before. The assembly of the electrochemical cell was completed by placing SS plungers in contact with both current collectors, and inserted into a custom cell setup described in the main text. An external pressure of 10 MPa was applied to this cell stack assembly by means of a screw tightened to an appropriate torque using a torque wrench.

All materials were handled and sample stacks assembled in a high purity Ar-filled glovebox maintained at $\sim$4 mbar positive pressure containing <0.1 ppm of H$_2$O and <0.1 ppm of O$_2$.

XPS Analysis

X-ray photoemission spectroscopy (XPS) was conducted using a PHI Versaprobe III XPS system generating focused, monochromatic $Al_{K\alpha}$ X-rays at 1486.6 eV, under ultrahigh vacuum (UHV) conditions with the main chamber maintained at pressures between $\sim$10^{-7}-10^{-6} Pa. The X-ray monochromator was operated at a power of 25W and an electron beam voltage of 15 kV. The instrument is equipped with dual beam charge neutralisation

8

capabilities - a low energy BaO electron source (beam diameter ∼5mm) and a low energy Ar^+ ion source. Samples were transferred from a glovebox into the XPS chamber using a vacuum transfer vessel to avoid contamination and any ambient exposures. Survey scans were acquired at pass energies of 224 eV, whereas for core-level spectra, a lower pass energy of 55 eV was used. For operando XPS experiments, all scans for survey and core-level spectra were acquired with both neutralisers switched off. Acquired spectra were then fitted to Gaussian-Lorentzian and Voigt lineshapes (or Doniach-Sunjic lineshapes for metallic Li components, where asymmetry was found to be significant), after application of a Shirley background, using CasaXPS software.[43] All spectra were then charge referenced to adventitious C at 284.8 eV through acquired C 1s spectra, and validated with that of Cl 2p spectra for Cl $2p_{3/2}$ = 198.5 eV, since Cl 2p signal remains unchanged throughout the Li plating process.[12, 20] Following this, fitted regions were quantified and used for estimating relative fractions of components therein.

Operando virtual electrode plating

"Virtual electrode plating" was conducted by alternating spectra acquisitions with exposure of the sample stack surface to the low energy electron beam. The electron dose was further modulated by adjusting the beam current between 2.5 µA and 30 µA, with the latter being the highest current for safe and stable operation of the neutraliser filament. During the operando XPS experiment, Ar^+ charge neutralisation was turned off.

Electrochemical measurements in cells with lithium-free anode

Electrochemical impedance spectroscopy (EIS), open circuit potential (OCP) and galvanostatic plating/stripping measurements were performed on cell stacks that were assembled within a PEEK mould into a custom cell setup in a manner described previously. The cells were connected in two-probe configuration to a Gamry Instruments Interface-1000 potentiostat for this purpose. EIS measurements were conducted in the frequency range of 1 MHz to 0.1 Hz with a voltage amplitude of 10 mV. Fitting of EIS data was done using the Z fit functionality in EC-lab® software v11.33 using the equivalent circuit as described in the main text. The EIS curves obtained were fitted to an equivalent circuit

as schematically depicted in Figure 4a. This circuit consists of a single resistor in series with three parallel circuits of a resistor and a constant-phase element (CPE) along with an additional Warburg diffusion component. Schlenker et al. attribute the inclusion of the latter to an impedance at low frequencies arising from a lithium vacancy diffusion gradient generated most likely at the interface between the LiIn and LPSCl.[38] In this equivalent circuit, one of the parallel circuits (R_2||CPE_2) in combination with the individual resistor R_1 can be assigned to the bulk and grain boundary resistance, which typically exhibit low capacities. The other circuit element pairs (R_3||CPE_3 and R_4||CPE_4) exhibiting relatively higher capacities can be understood to represent the LPSCl-Li interface and charge transfer (CT) processes respectively, as plating begins with the formation of an SEI.[37–39]

Competing Interests

The authors declare no competing interests.

References

1. Manthiram, A., Yu, X. & Wang, S. Lithium battery chemistries enabled by solid-state electrolytes. *Nature Reviews Materials* **2,** 1–16 (2017).

2. Pasta, M. *et al.* 2020 roadmap on solid-state batteries. *Journal of Physics: Energy* **2,** 032008 (2020).

3. Wu, C. *et al.* Current status and future directions of all-solid-state batteries with lithium metal anodes, sulfide electrolytes, and layered transition metal oxide cathodes. *Nano Energy* **87,** 106081 (2021).

4. Janek, J. & Zeier, W. G. A solid future for battery development. *Nature Energy* **1,** 16141 (2016).

5. Wu, X. *et al.* Operando Visualization of Morphological Dynamics in All-Solid-State Batteries. *Advanced Energy Materials* **9,** 1901547 (2019).

6. Hatzell, K. B. *et al.* Challenges in Lithium Metal Anodes for Solid-State Batteries. *ACS Energy Letters* **5,** 922–934 (3 2020).

7. Krauskopf, T., Richter, F. H., Zeier, W. G. & Janek, J. Physicochemical Concepts of the Lithium Metal Anode in Solid-State Batteries. *Chemical Reviews* **120,** 7745–7794 (2020).

8. Tang, Y. *et al.* Electro-chemo-mechanics of lithium in solid state lithium metal batteries. *Energy & Environmental Science* **14,** 602–642 (2021).

9. Narayanan, S., Gibson, J. S., Aspinall, J., Weatherup, R. S. & Pasta, M. In situ and operando characterisation of Li metal – Solid electrolyte interfaces. *Current Opinion in Solid State and Materials Science* **26,** 100978 (2 2022).

10. Richards, W. D., Miara, L. J., Wang, Y., Kim, J. C. & Ceder, G. Interface Stability in Solid-State Batteries. *Chemistry of Materials* **28,** 266–273 (1 2016).

11. Banerjee, A., Wang, X., Fang, C., Wu, E. A. & Meng, Y. S. Interfaces and Interphases in All-Solid-State Batteries with Inorganic Solid Electrolytes. *Chemical Reviews* **120,** 6878–6933 (14 2020).

12. Wenzel, S., Sedlmaier, S. J., Dietrich, C., Zeier, W. G. & Janek, J. Interfacial reactivity and interphase growth of argyrodite solid electrolytes at lithium metal electrodes. *Solid State Ionics* **318,** 102–112 (2018).

13. Yu, C. *et al.* Accessing the bottleneck in all-solid state batteries, lithium-ion transport over the solid-electrolyte-electrode interface. *Nature Communications* **8,** 1086 (1 2017).

14. Kato, Y. *et al.* High-power all-solid-state batteries using sulfide superionic conductors. *Nature Energy* **1,** 16030 (4 2016).

15. Nazri, G. Preparation, structure and ionic conductivity of lithium phosphide. *Solid State Ionics* **34,** 97–102 (1-2 1989).

16. Lin, Z., Liu, Z., Dudney, N. J. & Liang, C. Lithium Superionic Sulfide Cathode for All-Solid Lithium–Sulfur Batteries. *ACS Nano* **7,** 2829–2833 (3 2013).

17. Court-Castagnet, R., Kaps, C., Cros, C. & Hagenmuller, P. Ionic conductivity-enhancement of LiCl by homogeneous and heterogeneous dopings. *Solid State Ionics* **61,** 327–334 (1993).

18. Tan, D. H. S. *et al.* Elucidating Reversible Electrochemical Redox of Li_6PS_5Cl Solid Electrolyte. *ACS Energy Letters* **4,** 2418–2427 (10 2019).

19. Schwietert, T. K. *et al.* Clarifying the relationship between redox activity and electrochemical stability in solid electrolytes. *Nature Materials* **19,** 428–435 (4 2020).

20. Wood, K. N. *et al.* Operando X-ray photoelectron spectroscopy of solid electrolyte interphase formation and evolution in Li2S-P2S5 solid-state electrolytes. *Nature Communications* **9,** 1–10 (2018).

21. Wu, N. *et al.* In Situ Formation of Li3P Layer Enables Fast Li+ Conduction across Li/Solid Polymer Electrolyte Interface. *Advanced Functional Materials* **30,** 1–6 (2020).

22. Santhosha, A. L., Medenbach, L., Buchheim, J. R. & Adelhelm, P. The IndiumLithium Electrode in Solid-State Lithium-Ion Batteries: Phase Formation, Redox Potentials, and Interface Stability. *Batteries & Supercaps* **2,** 524–529 (2019).

23. Doux, J. M. *et al.* Stack Pressure Considerations for Room-Temperature All-Solid-State Lithium Metal Batteries. *Advanced Energy Materials* **10,** 1–6 (2020).

24. Davis, A. L. *et al.* Electro-chemo-mechanical evolution of sulfide solid electrolyte/Li metal interfaces: operando analysis and ALD interlayer effects. *Journal of Materials Chemistry A* **8,** 6291–6302 (2020).

25. Parejiya, A. *et al.* Improving Contact Impedance via Electrochemical Pulses Applied to Lithium–Solid Electrolyte Interface in Solid-State Batteries. *ACS Energy Letters,* 3669–3675 (2021).

26. Zhu, Y., He, X. & Mo, Y. Origin of Outstanding Stability in the Lithium Solid Electrolyte Materials: Insights from Thermodynamic Analyses Based on First-Principles Calculations. *ACS Applied Materials and Interfaces* **7,** 23685–23693 (42 2015).

27. Krauskopf, T. *et al.* The Fast Charge Transfer Kinetics of the Lithium Metal Anode on the Garnet-Type Solid Electrolyte Li 6.25 Al 0.25 La 3 Zr 2 O 12. *Advanced Energy Materials* **10,** 2000945 (27 2020).

28. Albertus, P. *et al.* Challenges for and Pathways toward Li-Metal-Based All-Solid-State Batteries. *ACS Energy Letters,* 1399–1404 (2021).

29. Wang, M. J., Carmona, E., Gupta, A., Albertus, P. & Sakamoto, J. Enabling "lithium-free" manufacturing of pure lithium metal solid-state batteries through in situ plating. *Nature Communications* **11,** 5201 (2020).

30. Connell, J. G. *et al.* Kinetic versus Thermodynamic Stability of LLZO in Contact with Lithium Metal. *Chemistry of Materials* **32,** 10207–10215 (2020).

31. Davis, A. L., Kazyak, E., Liao, D. W., Wood, K. N. & Dasgupta, N. P. Operando Analysis of Interphase Dynamics in Anode-Free Solid-State Batteries with Sulfide Electrolytes. *Journal of The Electrochemical Society* **168,** 070557 (2021).

32. Wenzel, S. *et al.* Interphase formation and degradation of charge transfer kinetics between a lithium metal anode and highly crystalline Li7P3S11 solid electrolyte. *Solid State Ionics* **286,** 24–33 (2016).

33. Wood, K. N. & Teeter, G. XPS on Li-Battery-Related Compounds: Analysis of Inorganic SEI Phases and a Methodology for Charge Correction. *ACS Applied Energy Materials* **1,** 4493–4504 (2018).

34. Gibson, J. *et al.* Gently Does It!: In Situ Preparation of Alkali Metal - Solid Electrolyte Interfaces for Photoelectron Spectroscopy. *Faraday Discussions* (2022).

35. Hakari, T. *et al.* Structural and Electronic-State Changes of a Sulfide Solid Electrolyte during the Li Deinsertion-Insertion Processes. *Chemistry of Materials* **29,** 4768–4774 (2017).

36. Vadhva, P. *et al.* Electrochemical Impedance Spectroscopy for All-Solid-State Batteries: Theory, Methods and Future Outlook. *ChemElectroChem* **8,** 1930–1947 (11 2021).

37. Kasemchainan, J. *et al.* Critical stripping current leads to dendrite formation on plating in lithium anode solid electrolyte cells. *Nature Materials* **18,** 1105–1111 (2019).

38. Schlenker, R. *et al.* Understanding the Lifetime of Battery Cells Based on Solid-State Li6PS5Cl Electrolyte Paired with Lithium Metal Electrode. *ACS Applied Materials and Interfaces* **12,** 20012–20025 (2020).

39. Zhang, W. *et al.* Interfacial Processes and Influence of Composite Cathode Microstructure Controlling the Performance of All-Solid-State Lithium Batteries. *ACS Applied Materials and Interfaces* **9,** 17835–17845 (2017).

40. Lu, Y. *et al.* Critical Current Density in Solid-State Lithium Metal Batteries: Mechanism, Influences, and Strategies. *Advanced Functional Materials* **2009925,** 1–33 (2021).

41. Liu, Y. *et al.* Insight into the Critical Role of Exchange Current Density on Electrodeposition Behavior of Lithium Metal. *Advanced Science* **8,** 2003301 (2021).

42. Pei, A., Zheng, G., Shi, F., Li, Y. & Cui, Y. Nanoscale Nucleation and Growth of Electrodeposited Lithium Metal. *Nano Letters* **17,** 1132–1139 (2 2017).

43. Fairley, N. *et al.* Systematic and collaborative approach to problem solving using X-ray photoelectron spectroscopy. *Applied Surface Science Advances* **5,** 100112 (2021).